APPLIED PHYSICS

Copyright © 2020 The Authors, some rights reserved; exclusive licensee American Association for the Advancement of Science. No claim to original U.S. Government Works. Distributed under a Creative Commons Attribution NonCommercial License 4.0 (CC BY-NC).

Optothermotronic effect as an ultrasensitive thermal sensing technology for solid-state electronics

T. Dinh[1,2]*, T. Nguyen[1], A. R. M. Foisal[1], H.-P. Phan[1], T.-K. Nguyen[1], N.-T. Nguyen[1], D. V. Dao[1,3]

The thermal excitation, regulation, and detection of charge carriers in solid-state electronics have attracted great attention toward high-performance sensing applications but still face major challenges. Manipulating thermal excitation and transport of charge carriers in nanoheterostructures, we report a giant temperature sensing effect in semiconductor nanofilms via optoelectronic coupling, termed optothermotronics. A gradient of charge carriers in the nanofilms under nonuniform light illumination is coupled with an electric tuning current to enhance the performance of the thermal sensing effect. As a proof of concept, we used silicon carbide (SiC) nanofilms that form nanoheterostructures on silicon (Si). The sensing performance based on the thermal excitation of charge carriers in SiC is enhanced by at least 100 times through photon excitation, with a giant temperature coefficient of resistance (TCR) of up to −50%/K. Our findings could be used to substantially enhance the thermal sensing performance of solid-state electronics beyond the present sensing technologies.

Downloaded from http://advances.sciencemag.org/ on June 23, 2020

INTRODUCTION

Detection and mediation of temperature are of considerable interest in industrial processes (*1*), laboratory (*2*), as well as daily life activities (*3*, *4*). Over the past century, tremendous progress has been made in the development and commercialization of temperature sensing devices, including resistive temperature detectors (RTDs) (*5*) and thermistors (*6*, *7*). These devices use the electrical resistance change versus temperature variation to define temperature coefficient of resistance (TCR) as an indicator for temperature sensitivity (*8*). TCR-based temperature sensing devices become popular, owing to their simplicity in design, fabrication, and implementation (*8*, *9*). Currently, RTD sensors are one of the main products of the current temperature sensing market. Nevertheless, these sensing technologies are fundamentally based on the nature of lattice scattering phenomena and/or thermal excitation of charge carriers, which limit their sensing performance (*10*, *11*). For example, the sensitivity of traditional thermal detectors is relatively low with a typical TCR value below 0.7%/K. The wide range of thermal sensing applications demands for the development of advanced technologies, which can substantially enhance the sensing performance of conventional solid-state devices by manipulating the generation and transport of charge carriers (*12*–*14*).

Several strategies have been proposed to enhance the temperature sensitivity (e.g., TCR) of conventional sensing materials and solid-state electronic devices (*15*–*18*). The modification of surface roughness in p-type silicon (p-Si) with gold nanoparticles (Au-NPs) can increase the temperature sensitivity up to 100% (*16*). This sensing concept could be suitable for electronic applications in liquid helium and cryogenic temperatures (e.g., 10 to 30 K). In nanocomposites, the alternation of tunneling distance between conductive nanotubes by volume phase transition could cause a large TCR value at elevated temperatures. At a volume phase transition temperature where the volume increases substantially, electrons require a higher energy to pass through the barrier, resulting in a substantial decrease in electrical conductivity (*15*). However, volume expansions or phase changes are limited at a specific temperature and certain conditions, posing a barrier for practical sensing applications.

Currently, generation and modulation of the thermally excited charge carriers have faced great challenges. For instance, thermal excitation occurs at near room temperature, while the doping concentration of charge carriers limits the excitation rate as well as the sensing performance of solid-sate electronics (*19*, *20*). Therefore, the temperature sensitivity of thermal devices is typically limited at 0.7%/K (*8*). While photon excitation by nonuniform light illumination contributes a gradient of charge carriers to the thermal excitation process, an electric field regulates the transport of these carriers. Thus, temperature sensitivity (TCR) can be appreciably modulated. This effect, termed the optothermotronic effect, reflects the coupling of a photovoltaic gradient and electric current to modulate the thermal excitation phenomenon.

In this work, we demonstrate the optothermotronic effect induced in solid-state electronics that has a lateral photovoltaic effect in nanoheterostructures. As proof of principle, we found the optothermotronic effect in highly doped p-type silicon carbide nanofilms grown on low-doped p-type silicon substrates (p^+-SiC/p-Si). We demonstrate a giant TCR of −50%/K in the SiC nanofilms by manipulating the optothermotronic effect. The high sensitivity is achieved at room temperature and above rather than requiring low operating temperatures (*16*). A nonuniform light illumination was used to generate a gradient of charge carriers. The formation of quasi-Fermi levels in Si and SiC under the light gradient, the thermal excitation, the photoexcitation of charge carriers, and the manipulation of SiC band energy under electric field are all attributed to the tunable optothermotronic sensitivity. Apart from the high sensing performance, the use of the large bandgap nanofilm semiconductor (SiC) (*21*) coating on the substrate (Si) also provides a suitable material choice for solid-state electronics working under harsh conditions including corrosive environments, owing to its excellent chemical inertness. In addition, the performance of the sensing technology is two orders of magnitude higher than that of flexible systems and a factor of 2 greater than the best inorganic system based on single-wall carbon nanotubes (*22*), carbon

[1]Queensland Micro- and Nanotechnology Centre, Griffith University, Brisbane, Queensland, Australia. [2]School of Mechanical and Electrical Engineering, University of Southern Queensland, Toowoomba, Queensland, Australia. [3]School of Engineering and Built Environment, Griffith University, Gold Coast, Queensland, Australia.
*Corresponding author. Email: toan.dinh@griffith.eu.au, toan.dinh@usq.edu.au

nanotube composites (*23*), graphene (*4*), reduced graphene oxide (*3*), and others (*10*).

Figure 1A shows the schematic sketch of the proposed SiC/Si optothermotronic platform with the relevant physical phenomena. Light illumination brings photons to excite charge carriers in the SiC/Si heterostructure and the silicon substrate while the SiC nanofilm is visible-blind (*24*). The nonuniform light illumination induces a gradient of charge carrier concentration or voltage gradient between electrodes P and Q with a light intensity stronger at Q and weaker at P. Subsequently, temperature changes provide thermal energy to excite charge carriers from the acceptor level to the valance band (*25*). Coupling of photoexcitation and an electric tuning current in the SiC/Si platform enhances the carrier transport properties in SiC nanofilms. The use of semiconductor nanofilms with a large band energy gap (SiC) eliminates the excitation of charge carriers in the SiC layer by visible lights owing to its visible-blind properties (*24*).

To form SiC/Si heterostructures, we used a low-pressure chemical vapor deposition process to grow 280-nm-thick SiC nanofilms on a p-type low-doped (10^{14} cm^{-3}) Si substrate. In the in situ doping process, aluminum dopant was used in the form of a trimethylaluminum [$(CH_3)_3Al$, TMAl] precursor. A doping level of 5×10^{18} cm^{-3} was examined by the Hall measurement for the aluminum-doped SiC nanofilms. Details of the growth process and the fabrication of SiC devices are described in Materials and Methods.

RESULTS

Figure 1B shows the transmission electron microscopy (TEM) image of the cross-sectional area between SiC and Si, showing the crystallinity of SiC nanofilms that was also confirmed by the selected-area electron diffraction (SAED) measurements (Fig. 1C) (*26*). Figure 1D indicates the formation of SiC grown on Si by x-ray diffraction (XRD). Atomic force microscopy (AFM) and Raman characterization results are illustrated in fig. S1. We carried out the current-voltage (*I*-*V*) measurements in darkness and at room temperature for SiC nanofilms and SiC/Si heterostructures (fig. S2). The results indicated an excellent ohmic contact formed between the electrodes and SiC nanofilms.

Figure 2A shows a home-built experimental setup for the characterization of the thermoresistive effect in SiC nanofilms (i.e., the resistance changes with temperature variation in darkness) and the optothermotronic effect in p$^+$-SiC/p-Si under light illumination. In thermoresistive measurements, we used a heater in an enclosed chamber to control the device temperature. Figure 2 (B and C) shows the measurement results for the thermoresistive effect of SiC nanofilms in darkness. With a constant applied electrical current *I*, the measured voltage *V* decreased with increasing temperature, indicating a decrease of electrical resistance (Fig. 2C). This suggests the dominance of the excited charge carriers compared to the carrier-lattice scattering effect in the p$^+$-SiC nanofilm. At an applied current of $I = 340$ μA, the measured voltage decreases from 100 to 88 mV (Fig. 2B),

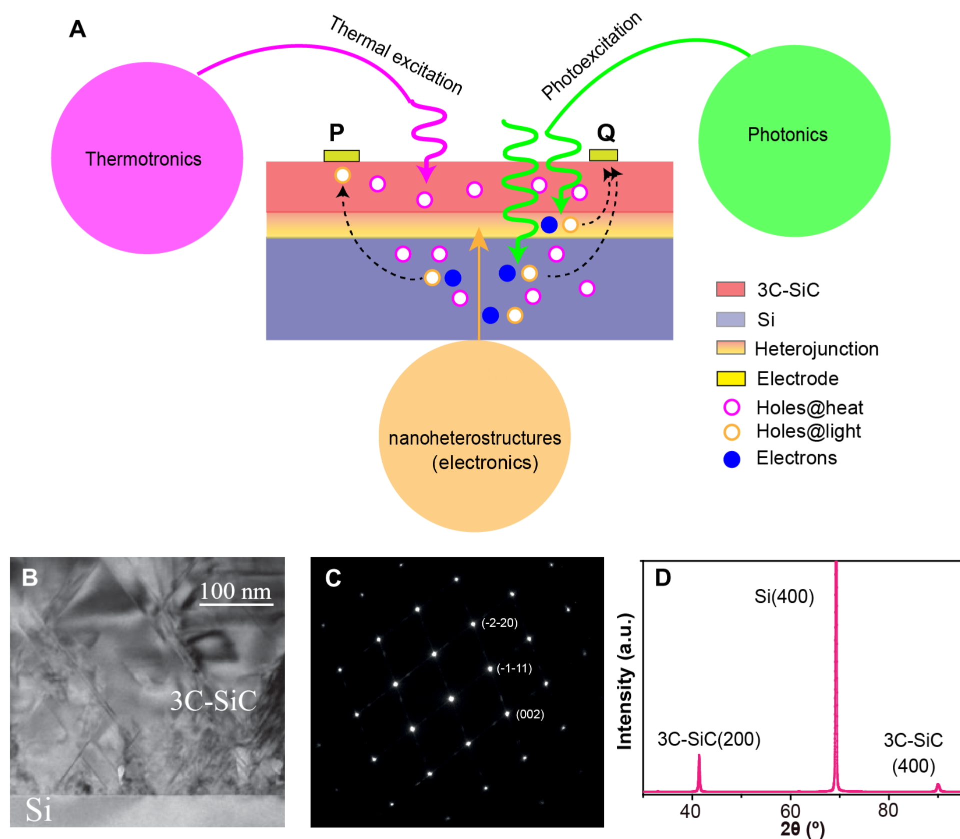

Fig. 1. Materials and concepts. (**A**) Diagram of optothermotronics that reflects the coupling of photon excitation, inducing a photovoltage in solid-state nanoheterostructures, and thermal excitation of charge carriers in semiconductor nanofilms. SiC nanofilms that formed a nanoheterostructure with Si are illustrated as an optothermotronic platform. (**B**) Cross-sectional TEM image of the as-fabricated SiC nanofilm constructed on Si. (**C**) SAED image of 3C-SiC. (**D**) XRD graph of the 3C-SiC film grown on Si. a.u., arbitrary units. Reprinted from (*26*), with the permission of AIP Publishing.

Downloaded from http://advances.sciencemag.org/ on June 23, 2020

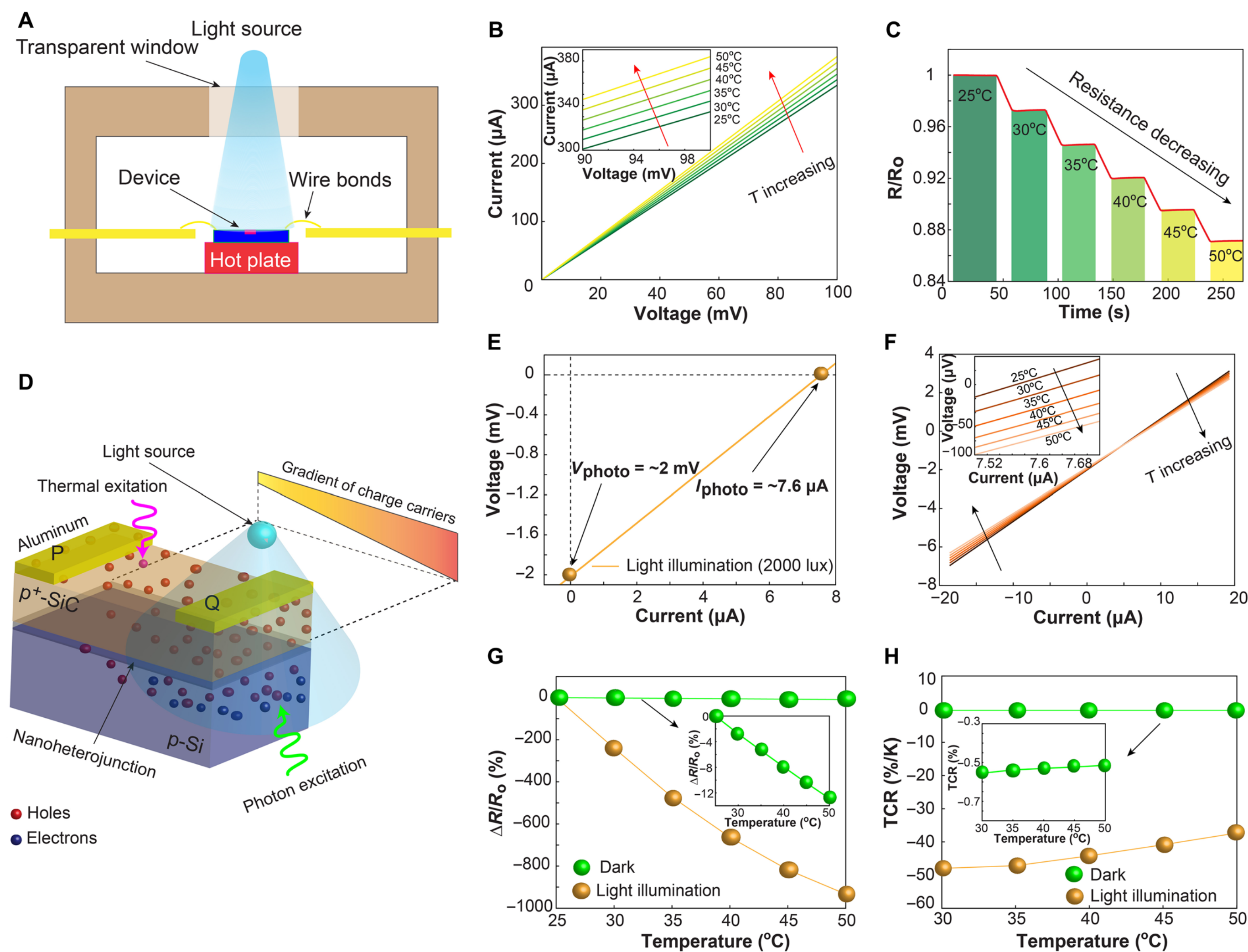

Fig. 2. Thermoresistance and optothermotronics. (**A**) Schematic sketch of the setup for characterization of thermoresistance and optothermotronics. (**B**) *I-V* characteristics of the SiC nanofilms under dark conditions. (**C**) Electrical resistance change with temperature variation. (**D**) Photoexcitation of the p^+-SiC/p-Si showing the nonuniform distribution of primary charge carriers in the SiC nanofilm under light illumination. Thermal excitation generates supplementary charge carriers by thermal energy, which is modulated by the gradient of the photogenerated primary charge carriers. (**E**) *I-V* characteristic of the SiC nanofilm under a light illumination of 2000 lux. The result indicated a photogenerated voltage of approximately 2 mV and a photocurrent of approximately 7.6 μA. (**F**) The *I-V* characteristics showing the change of the measured voltage with temperature variation. The inset illustrates the zoom-in graph of the *I-V* characteristics around 7.6 μA where the measured voltage changes notably. (**G**) Relative resistance change versus temperature under light illumination (2000 lux) and dark conditions at a constant current of 7.6 μA. (**H**) TCR of p^+-SiC/p-Si under dark conditions and under light illumination (2000 lux).

corresponding to a decrease of above 10% of the electrical resistance of p^+-SiC nanofilms (Fig. 2C). When the temperature increases, the acceptors in SiC are excited by the thermal energy and contribute to an increase in the conductivity or a decrease in the electrical resistance. On the basis of the linear *I-V* characteristics (Fig. 2B), the electrical resistance R is defined by Ohm's law: $R = V/I$, and the relative resistance change is simply described in the following form: $\Delta R/R_o = \Delta V/V_o$, where V_o and R_o are respectively the voltage and resistance measured at the reference temperature T_o; ΔV is the voltage change. In a narrow range of temperatures, the TCR can be approximated as $\mathrm{TCR} = \Delta R/R_o \times 1/\Delta T$, where $\Delta T = T - T_o$ is the temperature change. The TCR value was found to be almost constant at approximately −0.5%/K when the temperature changed from 25° to 50°C. This TCR value is well established for the current thermoresistive temperature sensing technologies using commercialized RTD sensors (*27*). To confirm that the TCR value of −0.5%/K is caused by only SiC layer, we controlled our experiment by transferring the SiC film onto an insulating substrate (glass). We carried out the experiments on temperature sensing properties of SiC on glass. The results indicate that the TCR value was about −0.5%/K (fig. S3), which is comparable with that observed for the SiC/Si platform in darkness. In the next section, we demonstrate the optothermotronic effect by coupling the photovoltaic effect and an optimal tuning current via the generation and control of charge carriers in p^+-SiC/p-Si.

Figure 2D shows our proposed concept for optothermotronics in p^+-SiC/p-Si under heat and light illumination. The nonuniform light introduces a gradient of charge carrier concentrations (i.e., holes)

Downloaded from http://advances.sciencemag.org/ on June 23, 2020

in the valance band of SiC (*28*). As such, the hole concentration increases from P toward Q, owing to a high intensity of light illumination at Q. Therefore, the quasi-Fermi level $E_{FV,SiC}$ of charge carriers at Q is closer to the valance band $E_{V,SiC}$ compared to that at P. This process results in an electric potential difference between P and Q. When the temperature increases, the acceptors in SiC are excited to the valance band of SiC, which are modulated by the potential difference between P and Q. To validate this concept, we illuminated an asymmetry gradient of light on the SiC nanofilm. The *I-V* measurements under a fixed light illumination of 2000 lux were performed, indicating a linear characteristic. At room temperature (25°C), the photovoltage V_{photo} was about 2 mV, and the generated photocurrent I_{photo} was approximately 7.6 μA (Fig. 2E). Figure 2F shows the full *I-V* measurement results under temperature variation. Close to the photocurrent of 7.6 μA, the measured voltage changed dramatically with increasing temperature (Fig. 2F, inset). This photocurrent was defined as an optimal current that is used to evaluate the sensitivity of the optothermotronic effect.

Figure 2(G and H) shows the relative resistance change versus temperature variation and TCR of p^+-SiC/p-Si under light illumination (2000 lux) compared with those measured under darkness. At 50°C, the relative resistance change under light conditions $(\Delta R/R_o)_{light}$ was measured with an increase of up to 1000% when the temperature increases from room temperature to 50°C. The increment of the resistance ratio between light and dark conditions $(\Delta R/R_o)_{light}/(\Delta R/R_o)_{dark}$ was observed to be approximately 100 times at 50°C (Fig. 2G). This enhancement reflects the important contribution of the photovoltage gradient generated in the SiC nanofilm under light illumination. The TCR value of SiC nanofilms was relatively stable at −0.5%/K for a temperature range from 25° to 50°C under dark conditions (Fig. 2H), while it increased approximately −50%/K under light conditions of 2000 lux and at an applied current of 7.6 μA. This increment indicates that the ultrasensitive temperature sensing effect of the p^+-SiC/p-Si platform is achievable by manipulating light conditions and electric field/current. The electrical potential and resistance can be photochemically modulated, suggesting other possible applications such as thermal refractive elements (*29*). The results demonstrate the remarkable advance of the temperature sensing technology using the lateral photoelectricity and thermal excitation of charge carriers in the nanoheterostructure.

To study the photo-excited charge effect on the performance of the optothermotronic device, we investigated the dependence of the TCR value on the light intensity and light position via the photovoltage V_{photo}. Figure 3A shows the increase of the photovoltage with increasing light intensity. At a low illumination intensity, the change of photovoltage exhibited a linear relationship with light intensity. Furthermore, the increment rate of the photovoltage decreases with increasing light intensity. This relationship is attributed to the saturation of the generation of electron-hole pairs (EHPs) under high light intensity exposure of the Si substrate and the SiC/Si heterojunction. Figure 3B shows the dependence of the photovoltage on the position of the light spot. The measured photovoltage was zero when the position of the light beam was in the middle between the two electrodes. The measured photovoltage increased with the light beam moving to the left (L) or right (R) electrodes. This phenomenon indicates that the largest gradient of charge carriers was achieved when the light beam shined directly at the electrodes. Figure 3C shows the dependence of the TCR value on the photovoltage induced by light intensity and position. The maxima of the TCR increase with increasing photovoltage in the range from 0 to 2 mV, and there is the saturation of the TCR with the increase of the normalized photovoltage in the range of 2 to 4 mV. The result indicates that the enhancement of the TCR value is governed by the increase in the gradient of number of charge carriers. Figure 3D shows the optothermotronic performance at high temperatures. The TCR value decreases with increasing temperature, e.g., from −50%/K at room temperature to approximately −10%/K at 350°C. This TCR is extremely high compared to that of other thermal detectors used for high-temperature applications (*8*, *10*, *11*, *19*, *20*). These results demonstrate the high potential of using optothermotronics for highly sensitive thermal sensing devices at high temperatures.

The optothermotronic effect showed a unique tunnelable and controllable property. In a range of applied currents either less than 5 μA or above 10 μA, the absolute TCR value was less than 1.5%/K (Fig. 4A), which is comparable with the stable TCR measured for the thermoresistive effect in darkness (Fig. 2H, inset). This is attributed to the dominance of the potential gradient generated by the photovoltaic effect compared with the opposite electric potential by injections ($I < 5$ μA), which is vice versa for $I > 10$ μA. The thermally excited charge carriers, therefore, play an insignificant role in temperature sensitivity. However, the applied current provides a sufficient compensation between the potential of photogenerated charge carriers and the injected electric potential, resulting in a small measured voltage in the current range of 5 to 10 μA. Figure S4 indicates the change of the electric current from 7.6 to 15.2 μA to achieve the maximum TCR value by controlling the gradient of photo-excited charges with a photovoltage changing from 2 to 4 mV. The charge carriers generated by thermal excitation create a large electric potential compared to the initial measured potential. Depending on the direction and value of the injected electrical potential, the thermally activated charge carriers can tune the TCR from positive to negative values. The highest negative TCR of up to −50%/K was observed (Fig. 4B). At the photocurrent, the total potential difference V_o is relatively small owing to the compensation of the photogenerated charge carrier potential and the injected electric potential. The charge carriers excited by the thermal energy will notably increase this potential difference (e.g., output voltage) under the application of the injected current. Therefore, the ultrahigh sensing performance with tenability was achieved for the p^+-SiC/p-Si platform under light illumination. The implementation of our TCR element in a tunable sensor could be highly valuable for the broad range of applications in lighting technology.

DISCUSSION

The enhancement of the photovoltage generated in optothermotronic devices depends on the following parameters: (i) absorption coefficient of photons, (ii) number of generated EHP, and (iii) collection of charge carriers at the electrodes, which is tailored by the transfer process of charge carriers between the SiC and Si interface. Figure 5A shows the charge distribution at the p^+-SiC/p-Si interface and the band energy diagram. Owing to a high hole doping concentration of 5×10^{18} cm^{-3}, holes from p^+-SiC diffuse to p-Si with a lower doping concentration of 10^{14} cm^{-3} and leave a negative charge on the SiC side of the heterojunction. Electrons as minor carriers in p-Si having a higher concentration move toward p^+-SiC and generate a positive charge on the Si side of the heterojunction, creating an electric field E_o. This electric field bends the valence band of p^+-SiC

Downloaded from http://advances.sciencemag.org/ on June 23, 2020

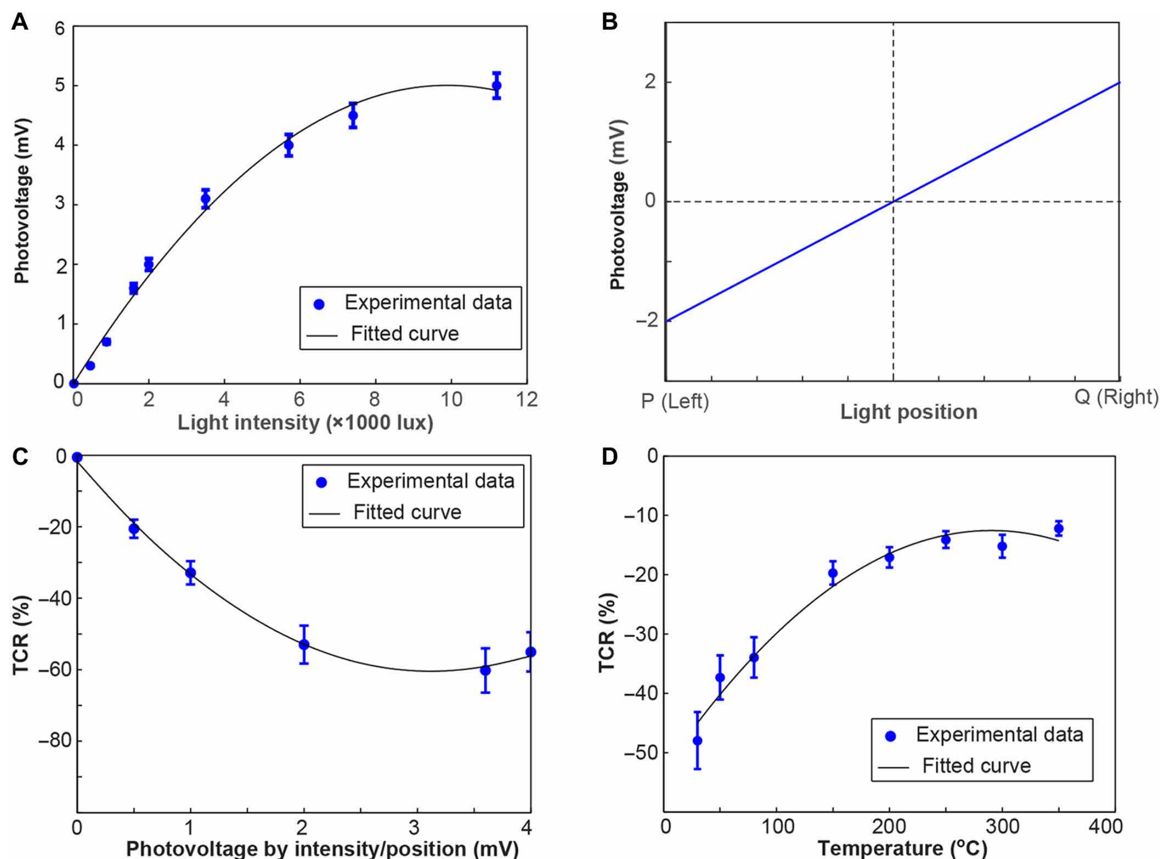

Fig. 3. Impact of photovoltage and high temperatures on TCR. (**A**) Photovoltage versus light intensity. (**B**) Photovoltage versus light position. (**C**) TCR versus photovoltage by changing light intensity and position. (**D**) TCR measured at high temperatures.

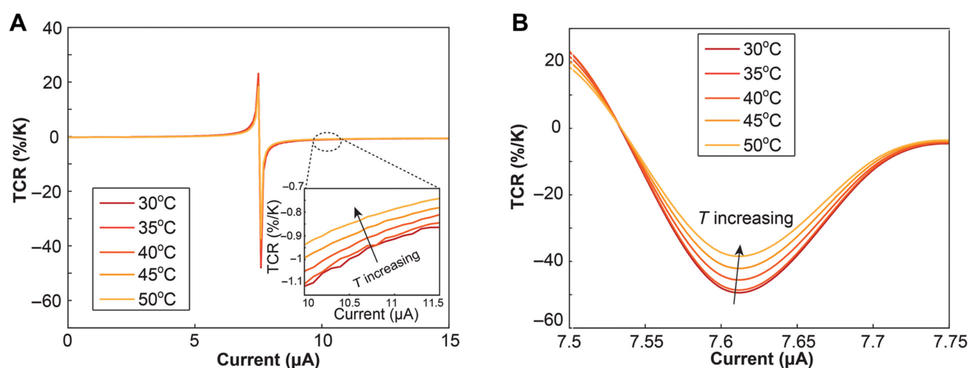

Fig. 4. Tunable optothermotronics. (**A**) The dependence of TCR on applied currents under light illumination. (**B**) Zoom-in TCR of p$^+$-SiC/p-Si around a photocurrent of 7.6 μA.

upward with respect to that of p-Si. The formation of the band energy diagram in Fig. 5A is based on the conduction band offset of $E_C = 0.45$ eV and the valance band offset of $E_V = 1.7$ eV between SiC and Si (*30*, *31*). With a large bandgap of 2.3 eV, SiC showed insignificant absorption. As such, we transferred the SiC nanofilms to a glass substrate and measured the SiC resistance under the illumination of the different wavelengths from ultraviolet (UV) to visible light (e.g., 375, 521, and 637 nm). The change of the SiC resistance was measured to be small. Under visible light illumination, the photogenerated EHPs appear in the heterojunction and the silicon layer. The holes and electrons that do not combine will contribute to the conductivity. Because of the nonequilibrium conditions under light illumination, the Fermi level E_F splits into two quasi-Fermi levels (e.g., E_{FC} for electrons and E_{FV} for holes), creating a chemical energy eV = $E_{FC} - E_{FV}$. Because of the large concentration of holes in p-type Si and SiC, the gradient of the Fermi energy for the valance band E_{FV} is smaller than the gradient of E_{FC} (Fig. 5B). Since p-Si initially has a lower hole concentration than p$^+$-SiC, the photogenerated holes push the

Downloaded from http://advances.sciencemag.org/ on June 23, 2020

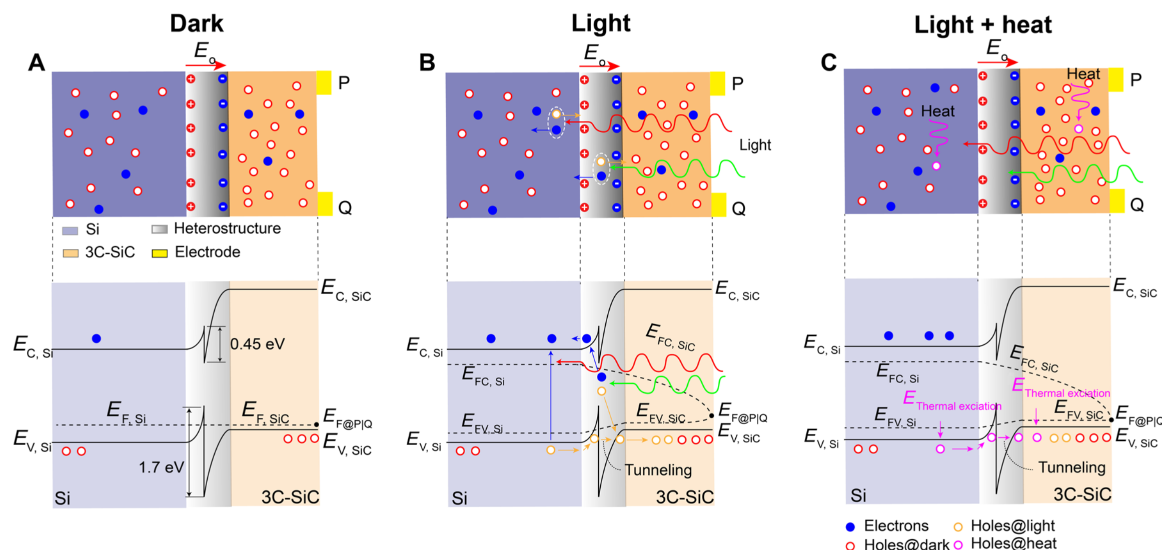

Fig. 5. Photoexcitation and thermal excitation in p⁺-SiC/p-Si. (**A**) Charge distribution and band diagram of SiC/Si heterojunctions under dark conditions. (**B**) EHP generation and transport in the SiC/Si heterojunction under light illumination. (**C**) Thermally excited carriers and transport by thermal energy.

Fermi energy $E_{FV,Si}$ more notably toward the valance band $E_{V,Si}$ compared to the shift of $E_{FV,SiC}$ toward $E_{V,SiC}$. This leads to a potential difference between Si and SiC (i.e., $E_{FV,Si} - E_{FV,SiC}$) (*32*, *33*). The built-in electric field E_o, creating a driving force, separates the EHP and drives the photogenerated holes in the heterostructure toward p^+-SiC and photogenerated electrons toward p-Si. In the SiC layer, these holes flow toward the right (e.g., at electrode P or Q) because the electrochemical potential decreases toward the right. Because of the strong recombination at the surface/electrode, the Fermi energies merge into a single Fermi energy (at P and Q). When the temperature increases, the acceptors are excited by thermal energy and contribute the charge carriers in the valance band (Fig. 5C). For example, thermal energy excites charge carriers in both SiC and Si layers. At a low temperature range, e.g., below 100°C, only a small number of charge carriers migrate to SiC via tunneling mechanism, and the current between SiC and Si was measured to be small (fig. S5). Therefore, the contribution of charge carriers from Si is insignificant at low temperatures. At a high temperature range of above 100°C, thermally excited charge carriers from Si can migrate to SiC via thermionic emission and tunneling. Consequently, the current from Si to SiC becomes important at high temperatures, and the thermally excited charges from Si have a more important influence on the TCR enhancement. We hypothesize that thermally generated holes in p-Si can be driven toward p^+-SiC by the built-in electric field E_o and via a tunneling mechanism. We believe that photogenerated EHP can also be generated in SiC films. However, the number of EHPs generated in SiC is expected to be smaller than that generated in Si due to the insignificant absorption of SiC films to visible light. Depending on the light and heat conditions, the width of the depletion region can vary, leading to the carrier transfer through tunneling from Si to 3C-SiC and vice versa. Under a low intensity of light and at low temperatures, the diode configuration of the 3C-SiC/Si heterojunction allows the charge carriers to move from Si to SiC, whenever there are excessive charge carriers in Si (e.g., by photon excitation). The possibility of charge carriers to move in the reverse direction (e.g., through tunneling) is smaller compared to the forward direction (fig. S6). Nonuniform light illumination induces a gradient of these photo-excited charges, i.e., the photovoltage, which is coupled with the electric current to control the voltage V_o and enhance the TCR value. Figure 6 illustrates the concept of tunneled charge carriers coupled with tuning current to enhance the sensing performance.

Under nonuniform light illumination, the hole concentration at electrode Q is higher than that at P, forming a gradient of charge carriers or photovoltage $V_{photo} = E_{FV,SiC@P} - E_{FV,SiC@Q}$ (Fig. 6A, left). Figure 6B shows this lateral photovoltage V_{photo} measured in real time under ON/OFF state of a light illumination of 2000 lux, showing the repeatability and reliability of the signal. The response time to the light illumination was estimated to be less than 50 ms, corresponding to a switching frequency of above 20 Hz (fig. S7). This is a relatively fast response compared to that of other thermal devices with a typical response time of a few seconds (*22*). The value of V_{photo} decreased with increasing temperature at a rate of 0.2%/K (Fig. 6C). This indicates that the chemical energy decreases with increasing temperature. The decrease of the energy barrier height between p-Si and p^+-SiC could be attributed to the reduction of the Fermi energy difference between p-Si and p^+-SiC. The photovoltage induces a charge current, which is defined by Fick's law of diffusion (*33*) $j_d = -e \times n \times D \times \text{grad}(n)/n$, where e and n are the elementary charge and the charge concentration, respectively; D is the diffusion coefficient depending on the carrier mobility.

By applying a bias/field current from P to Q (i.e., a negative potential placed at Q), the SiC band energy is bent upward from P to Q. This bias current corresponds to an electric field $E = -\text{grad}(\varphi)$, where φ is the electric potential that drives a field current j_f in the reverse direction of the diffusion current j_d, which is expressed as (*24*, *34*) $j_f = \sigma/e \times \text{grad}(e\varphi)$, where σ is the conductivity of the charge carriers. Therefore, the field current compensates for the diffusion current, resulting in a relatively small electric field in total, which was measured as V_o. Figure 6A (middle) shows this potential difference V_o induced between two electrodes P and Q at room temperature (25°C). If the temperature increases, the thermal excitation of holes will notably increase the conductivity of the charge carriers. The TCR depends on the change of the measured voltage TCR = $(V - V_o)/V_o \times 1/\Delta T$, where V and V_o are the measured voltage at

Downloaded from http://advances.sciencemag.org/ on June 23, 2020

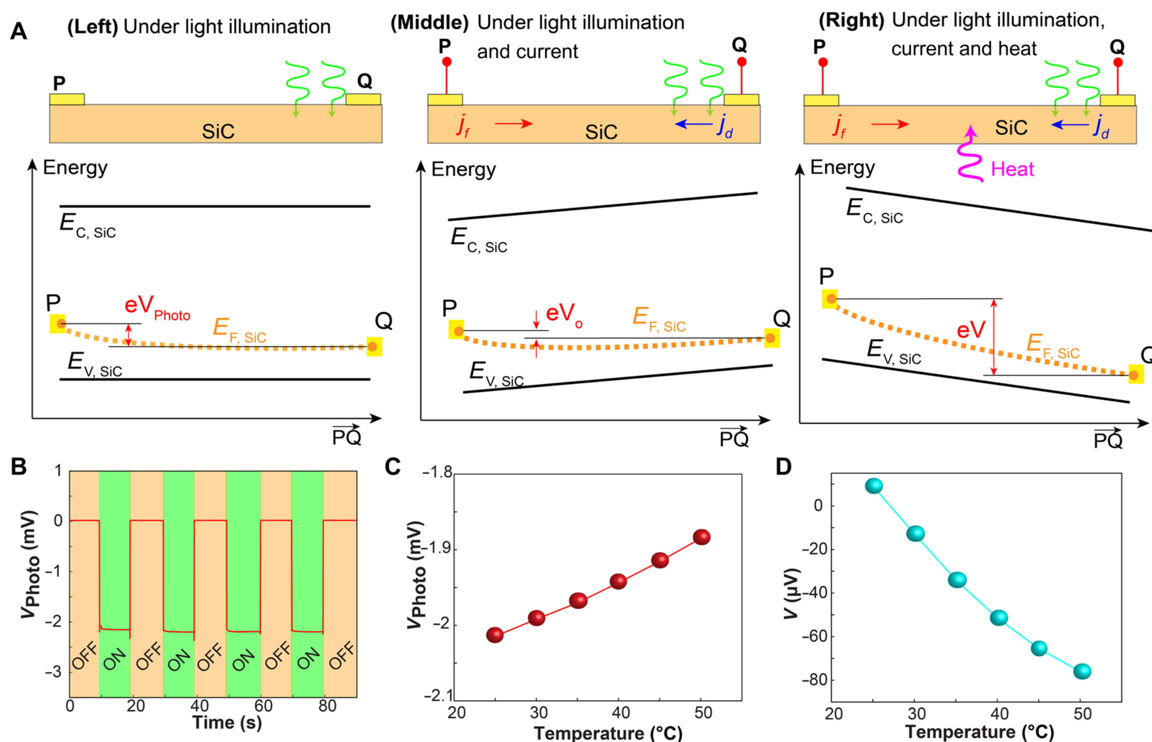

Fig. 6. Modulation of optothermotronic potential. (**A**) (Left) Energy band diagram of p^+-SiC showing the lateral photovoltage between two electrodes. (Middle) Energy band diagram of p^+-SiC showing the small electric potential under nonuniform light illumination and a tuning current. (Right) Energy band diagram showing the shift of the electric potential with the thermal excitation. (**B**) Photogenerated voltage measured under 2000-lux light illumination. Four cycles of ON and OFF states showing the repeatability of the lateral photovoltage. (**C**) The dependence of the photovoltage on the temperature variation. (**D**) The measured electric potential versus temperature variation.

temperature T and room temperature T_o, respectively (Fig. 6A). The measured V_o depends on the difference of the Fermi levels between P and Q (Fig. 6A, middle). Under the application of the bias/field current, the thermal excitation of charge carriers tends to bend the SiC band energy downward from P to Q (Fig. 6A, right). If the field current is smaller than the diffused current, the potential at P is higher than that at Q, resulting in a positive TCR and vice versa. Figure 6D shows the experimental results on the change of the measured voltage between terminals P and Q with increasing temperatures. The measured voltage changed by approximately 1000%, and its sign turned from positive to negative when the temperature increases from the room temperature to 50°C. For the positive TCR maxima, the initial Fermi level of P is higher than that of Q, resulting in a positive V_o. In this case, the absolute voltage difference $|V - V_o|$ is smaller than that of the negative TCR maxima as V_o is negative for the negative TCR maxima. Therefore, the positive TCR maxima shown in Fig. 4A are smaller than the negative TCR maxima. When the field current approaches the diffused current, the voltage V_o is relatively small. Therefore, the temperature changes cause the large difference between V and V_o (Fig. 6A), resulting in the maximum TCR (Fig. 4A). In addition, if the field current decreases and is smaller than the diffused current, the voltage V_o reduces, leading to a decreasing TCR value. The giant change successfully demonstrates optothermotronics as an advanced thermal sensing technology for solid-state electronics.

In addition, inhomogeneous irradiation has been achieved with an integrated light-emitting diode (LED) light source and is functional over a range of wavelengths. For instance, the experimental data showed that the device works properly with any wavelengths from UV (370 nm) to visible (780 nm) (fig. S8A). For implementation of optothermotronics, nonuniform light illumination can be consequently generated by the integration of a LED, including the green gallium nitride Al(Ga)N LED grown directly on SiC (fig. S8B) (*35*). In addition, our experimental data (fig. S9) indicated that the 3C-SiC/Si platform can harvest solar energy and function as a self-powered generation device, while the nonuniform light is simply implemented by a concentrating lens to focus the light photons on an electrode area of the device.

In conclusion, we demonstrated an ultrasensitive thermal sensing technology based on the optothermotronic effect in nanoheterostructures. Optothermotronics uses the coupling of the photon excitation in the p^+-SiC/p-Si heterostructure and the electric tuning current to manipulate the thermal excitation of charge carriers in SiC nanofilms, resulting in a giant temperature sensing effect. The optothermotronic effect is electrically controllable with the temperature sensitivity being tunable from negative TCR to positive TCR by compensating for the photogenerated hole gradient and the electric potential. We found a giant TCR value of approximately −50%/K by optoelectronic coupling, which is 100-fold larger than the TCR value measured in darkness and at least two orders of magnitude higher than the performance of current commercialized RTD sensors. Optothermotronics could be used to notably enhance the performance of solid-state electronics beyond the state-of-the-art thermal sensing technologies.

Downloaded from http://advances.sciencemag.org/ on June 23, 2020

MATERIALS AND METHODS

Growth of SiC nanofilms

A hot-wall low-pressure chemical vapor deposition reactor was used to grow single-crystalline 3C-SiC at 1000°C. To provide Si and C atoms for the growth process, we use silane (99.999%) and acetylene (99.999%) as precursors. The trimethylaluminum [$(CH_3)_3Al$, TMAl] precursor with an Al atomic concentration of above 10^{19} cm^{-3} was deployed to form p-type highly doped SiC materials in the in situ growth process.

Sample fabrication

Aluminum with a thickness of 300 nm was deposited on top of SiC wafer by a sputtering process. Next, a lithography process was performed with a 2-μm-thick positive photoresist layer spin-coated on the aluminum layer at a rotational speed of 4000 rpm. The wafer was then soft baked at 105°C for 90 s. The photoresist layer was patterned using UV light and a photoresist developer. A wet etching process was used to etch aluminum and form the electrodes. Last, the photoresist layer was removed.

Characterization and measurement

In an area of 5 by 5 μm^2, AFM measurements indicated a root mean square roughness of less than 20 nm (Supplementary Materials). The thickness of the SiC films was determined to be 280 nm by NanoSpec-based measurements with a nonuniformity across the as-grown SiC wafer within ±1%. Hall measurements were performed to determine the doping concentration of carriers in SiC films. TEM, SAED, and XRD measurement techniques were used to characterize the crystallinity of the SiC films grown on Si. Temperature characterization was performed using an enclosed Linkam chamber (HFS600E-PB4) and the light illumination at 2000 lux from a microscope. All electrical measurements including *I*-*V* characteristics were performed using a SourceMeter (Keithley 2450). The Joule heating effect was negligible as the electrical resistance was measured to be stable from a low supply current (100 nA) to more than 200 μA. Furthermore, we measured the surface temperature of the device with and without light illumination using an RTD. The resistance variation of the RTD sensor was relatively small (e.g., below 0.01%), indicating that the photothermal effect was also negligible.

SUPPLEMENTARY MATERIALS

Supplementary material for this article is available at http://advances.sciencemag.org/cgi/content/full/6/22/eaay2671/DC1

REFERENCES AND NOTES

1. A. Feteira, Negative Temperature Coefficient Resistance (NTCR) ceramic thermistors: An industrial perspective. *J. Am. Ceram. Soc.* **92**, 967–983 (2009).
2. C. Zhu, A. Chortos, Y. Wang, R. Pfattner, T. Lei, A. C. Hinckley, I. Pochorovski, X. Yan, J. W.-F. To, J. Y. Oh, J. Y. Oh, J. B.-H. Tok, Z. Bao, B. Murmann, Stretchable temperature-sensing circuits with strain suppression based on carbon nanotube transistors. *Nat. Electron.* **1**, 183–190 (2018).
3. T. Q. Trung, S. Ramasundaram, B.-U. Hwang, N.-E. Lee, An all-elastomeric transparent and stretchable temperature sensor for body-attachable wearable electronics. *Adv. Mater.* **28**, 502–509 (2016).
4. C. Yan, J. Wang, P. S. Lee, Stretchable graphene thermistor with tunable thermal index. *ACS Nano* **9**, 2130–2137 (2015).
5. V. K. Rai, Temperature sensors and optical sensors. *Appl. Phys. B* **88**, 297–303 (2007).
6. T. Q. Trung, H. S. Le, T. M. L. Dang, S. Ju, S. Y. Park, N.-E. Lee, Freestanding, fiber-based, wearable temperature sensor with tunable thermal index for healthcare monitoring. *Adv. Healthc. Mater.* **7**, 1800074 (2018).
7. T. Dinh, H.-P. Phan, T.-K. Nguyen, A. Qamar, A. R. M. Foisal, T. N. Viet, C.-D. Tran, Y. Zhu, N.-T. Nguyen, D. V. Dao, Environment-friendly carbon nanotube based flexible electronics for noninvasive and wearable healthcare. *J. Mater. Chem. C* **4**, 10061–10068 (2016).
8. T. Dinh, H.-P. Phan, A. Qamar, P. Woodfield, N.-T. Nguyen, D. V. Dao, Thermoresistive effect for advanced thermal sensors: Fundamentals, design considerations, and applications. *J. Microelectromech. S.* **26**, 966–986 (2017).
9. C. Yi, J.-H. Lee, B. S. Kwak, M. X. Lin, H. O. Kim, H.-I. Jung, Diagnosis of diabetes mellitus using sialic acid expression of erythrocyte and a microfluidic resistive temperature detector (micro-RTD). *Sens. Actuators B* **191**, 305–312 (2014).
10. S. Y. Hong, Y. H. Lee, H. Park, S. W. Jin, Y. R. Jeong, J. Yun, I. You, G. Zi, J. S. Ha, Stretchable active matrix temperature sensor array of polyaniline nanofibers for electronic skin. *Adv. Mater.* **28**, 930–935 (2016).
11. T.-P. Huynh, P. Sonar, H. Haick, Advanced materials for use in soft self-healing devices. *Adv. Mater.* **29**, 1604973 (2017).
12. N. S. Boltovets, V. V. Kholevchuk, R. V. Konakova, V. F. Mitin, E. F. Venger, Ge-film resistance and Si-based diode temperature microsensors for cryogenic applications. *Sensor. Actuat. A-Phys.* **92**, 191–196 (2001).
13. X. F. Zhou, H. Zhang, H. Yan, C. L. He, M. H. Lu, R. Y. Hao, *Giant* temperature coefficient of resistance in Co-doped ZnO thin films. *Appl. Phys. A* **114**, 809–812 (2014).
14. M. E. Itkis, F. Borondics, A. Yu, R. C. Haddon, Bolometric infrared photoresponse of suspended single-walled carbon nanotube films. *Science* **312**, 413–416 (2006).
15. G. E. Fernandes, J. H. Kim, A. K. Sood, J. Xu, Giant temperature coefficient of resistance in carbon nanotube/phase-change polymer nanocomposites. *Adv. Funct. Mater.* **23**, 4678–4683 (2013).
16. S.-H. Lee, S. Hwang, J.-W. Jang, Giant temperature coefficient of resistivity and cryogenic sensitivity in silicon with galvanically displaced gold nanoparticles in freeze-out region. *ACS Nano* **11**, 1572–1580 (2017).
17. F. Niklaus, C. Vieider, H. Jakobsen, paper presented at the *Mems/Moems Technologies and Applications III*, J. C. Chiao, X. Chen, Z. Zhou, X. Li, Eds. (Spie-Int. Soc. Optical Engineering, Bellingham, 2008), vol. 6836.
18. C. Boragno, U. Valbusa, G. Pignatel, Fast P-doped silicon bolometer for detecting heat pulses. *Appl. Phys. Lett.* **50**, 583–584 (1987).
19. T. Dinh, H. P. Phan, T. Kozeki, A. Qamar, T. Namazu, N. T. Nguyen, D. V. Dao, Thermoresistive properties of p-type 3C–SiC nanoscale thin films for high-temperature MEMS thermal-based sensors. *RSC Adv.* **42**, 106083 (2015).
20. T. Dinh, H.-P. Phan, D. V. Dao, P. Woodfield, A. Qamar, N.-T. Nguyen, Graphite on paper as material for sensitive thermoresistive sensors. *J. Mater. Chem. C* **3**, 8776–8779 (2015).
21. D. Nakamura, I. Gunjishima, S. Yamaguchi, T. Ito, A. Okamoto, H. Kondo, S. Onda, K. Takatori, Ultrahigh-quality silicon carbide single crystals. *Nature* **430**, 1009–1012 (2004).
22. H. Yang, D. Qi, Z. Liu, B. K. Chandran, T. Wang, J. Yu, X. Chen, Soft thermal sensor with mechanical adaptability. *Adv. Mater.* **28**, 9175–9181 (2016).
23. S. Harada, W. Honda, T. Arie, S. Akita, K. Takei, Fully printed, highly sensitive multifunctional artificial electronic whisker arrays integrated with strain and temperature sensors. *ACS Nano* **8**, 3921–3927 (2014).
24. A. R. M. Foisal, H.-P. Phan, T. Kozeki, T. Dinh, K. N. Tuan, A. Qamar, M. Lobino, T. Namazu, D. V. Dao, 3C–SiC on glass: An ideal platform for temperature sensors under visible light illumination. *RSC Adv.* **6**, 87124–87127 (2016).
25. S. M. Sze, K. K. Ng, *Physics of Semiconductor Devices* (John Wiley & Sons, 2006).
26. H.-P. Phan, D. V. Dao, P. Tanner, L. Wang, N.-T. Nguyen, Y. Zhu, S. Dimitrijev, Fundamental piezoresistive coefficients of p-type single crystalline 3C-SiC. *Appl. Phys. Lett.* **104**, 111905 (2014).
27. P. R. N. Childs, J. R. Greenwood, C. A. Long, Review of temperature measurement. *Rev. Sci. Instrum.* **71**, 2959 (2000).
28. I. K. Moon, B. Ki, S. Yoon, J. Oh, Lateral photovoltaic effect in flexible free-standing reduced graphene oxide film for self-powered position-sensitive detection. *Sci. Rep.* **6**, 33525 (2016).
29. P. Berto, L. Philippet, J. Osmond, C. F. Liu, A. Afridi, M. M. Marques, B. M. Agudo, G. Tessier, R. Quidant, Tunable and free-form planar optics. *Nat. Photonics* **13**, 649–656 (2019).
30. V. V. Afanas'ev, M. Bassler, G. Pensl, M. Schulz, E. S. von Kamienski, Band offsets and electronic structure of SiC/SiO_2 interfaces. *J. Appl. Phys.* **79**, 3108 (1996).
31. T. Dinh, H.-P. Phan, N. Kashaninejad, T.-K. Nguyen, D. V. Dao, N.-T. Nguyen, An on-chip sic mems device with integrated heating, sensing, and microfluidic cooling systems. *Adv. Mater. Interfaces* **5**, 1800764 (2018).
32. J. Nelson, *The Physics of Solar Cells* (Imperial College Press, 2003).
33. P. Wurfel, U. Wurfel, *Physics of Solar Cells: From Basic Principles to Advanced Concepts* (John Wiley & Sons, 2006).
34. U. Würfel, A. Cuevas, P. Würfel, Charge carrier separation in solar cells. *IEEE J. Photovoltaics* **5**, 461–469 (2015).
35. A. R. M. Foisal, T. Dinh, V. T. Nguyen, P. Tanner, H.-P. Phan, T.-K. Nguyen, B. Haylock, E. W. Streed, M. Lobino, D. V. Dao, Self-powered broadband (UV-NIR) photodetector based on 3C-SiC/Si heterojunction. *IEEE T. Electron Dev.* **66**, 1804–1809 (2019).
36. D. Massoubre, L. Wang, L. Hold, A. Fernandes, J. Chai, S. Dimitrijev, A. Iacopi, Vertically conductive Single-Crystal SiC-based Bragg reflector grown on Si wafer. *Sci. Rep.* **5**, 17026 (2015).

Downloaded from http://advances.sciencemag.org/ on June 23, 2020

Acknowledgments: The 3C-SiC material was developed and supplied by L. Hold and A. Iacopi of the Queensland Microtechnology Facility, part of the Queensland node—Griffith—of the Australian National Fabrication Facility. The epitaxial SiC deposition was developed as part of Griffith Universities Joint Development Agreement with SPT Microtechnology, the manufacturer of the Epix production reactor. **Funding:** This work has been partially supported by the Foundation for Australia-Japan Studies, Australian Research Council grants LP150100153 and LP160101553. The project "Superior Sensor Network (SSN) for Harsh Environments" was supported by the Foundation for Australia-Japan Studies under the Rio Tinto Australia-Japan Collaboration Project. **Author contributions:** D.V.D., N.-T.N., and T.D. conceived and supervised the project. Material preparation, fabrication, and characterization were carried out by T.D., T.N., and H.-P.P. T.D. and T.N. performed measurements with assistance from A.R.M.F. T.-K.N. contributed to sample fabrication. The manuscript was written by T.D. and with contributions from all authors. **Competing interests:** D.V.D., T.D., and T.N. are inventors on a patent application related to this work filed by Griffith University (no. 2023306, filed 13 June 2019). The authors declare that they have no other competing interests. **Data and materials availability:** All data needed to evaluate the conclusions in the paper are present in the paper and/or the Supplementary Materials. Additional data related to this paper may be requested from the authors.

Submitted 4 June 2019
Accepted 13 March 2020
Published 27 May 2020
10.1126/sciadv.aay2671

Citation: T. Dinh, T. Nguyen, A. R. M. Foisal, H.-P. Phan, T.-K. Nguyen, N.-T. Nguyen, D. V. Dao, Optothermotronic effect as an ultrasensitive thermal sensing technology for solid-state electronics. *Sci. Adv.* **6**, eaay2671 (2020).

Downloaded from http://advances.sciencemag.org/ on June 23, 2020

Science Advances

Optothermotronic effect as an ultrasensitive thermal sensing technology for solid-state electronics
T. Dinh, T. Nguyen, A. R. M. Foisal, H.-P. Phan, T.-K. Nguyen, N.-T. Nguyen and D. V. Dao

Sci Adv **6** (22), eaay2671.
DOI: 10.1126/sciadv.aay2671

ARTICLE TOOLS	http://advances.sciencemag.org/content/6/22/eaay2671
SUPPLEMENTARY MATERIALS	http://advances.sciencemag.org/content/suppl/2020/05/21/6.22.eaay2671.DC1
REFERENCES	This article cites 32 articles, 1 of which you can access for free http://advances.sciencemag.org/content/6/22/eaay2671#BIBL
PERMISSIONS	http://www.sciencemag.org/help/reprints-and-permissions

Use of this article is subject to the Terms of Service

Science Advances (ISSN 2375-2548) is published by the American Association for the Advancement of Science, 1200 New York Avenue NW, Washington, DC 20005. The title *Science Advances* is a registered trademark of AAAS.

Copyright © 2020 The Authors, some rights reserved; exclusive licensee American Association for the Advancement of Science. No claim to original U.S. Government Works. Distributed under a Creative Commons Attribution NonCommercial License 4.0 (CC BY-NC).

Downloaded from http://advances.sciencemag.org/ on June 23, 2020